

---

# Domain-decomposed Fully Coupled Implicit Methods for a Magnetohydrodynamics Problem\*

Serguei Ovtchinnikov<sup>1</sup>, Florin Dobrian<sup>2</sup>, Xiao-Chuan Cai<sup>3</sup>, David Keyes<sup>4</sup>

<sup>1</sup> University of Colorado at Boulder, Department of Computer Science, 430 UCB, Boulder, CO 80309, USA, [serguei.ovtchinnikov@colorado.edu](mailto:serguei.ovtchinnikov@colorado.edu)

<sup>2</sup> Old Dominion University, Department of Computer Science, 3300 ECS Building, Norfolk, VA 23529, USA, [dobrian@cs.odu.edu](mailto:dobrian@cs.odu.edu)

<sup>3</sup> University of Colorado at Boulder, Department of Computer Science, 430 UCB, Boulder, CO 80309, USA, [cai@cs.colorado.edu](mailto:cai@cs.colorado.edu)

<sup>4</sup> Columbia University, Department of Applied Physics & Applied Mathematics, 500 W. 120th St., New York, NY 10027, USA, [david.keyes@columbia.edu](mailto:david.keyes@columbia.edu)

We present a parallel fully coupled implicit Newton-Krylov-Schwarz algorithm for the numerical solution of the unsteady magnetic reconnection problem described by a system of reduced magnetohydrodynamics equations in two dimensions. In particular, we discuss the linear and nonlinear convergence and the parallel performance of a third-order implicit algorithm, and we compare our results with those obtained with an explicit method.

## 1 Introduction

In the magnetohydrodynamics (MHD) formalism plasma is treated as a conducting fluid satisfying the Navier-Stokes equations coupled with Maxwell's equations [6]. The behavior of an MHD system is complex since it admits phenomena such as Alfvén waves and their instabilities. One of the intrinsic features of MHD is the formation of a singular current density sheet, which is linked to the reconnection of magnetic field lines [3, 9, 10, 12], which in turn leads to the release of energy stored in the magnetic field. Numerical simulation of the reconnection plays an important role in our understanding of physical systems ranging from the solar corona to laboratory fusion devices. Capturing the change of the magnetic field topology requires a more general model than ideal MHD. A resistive MHD system is considered in this paper. To simulate this multi-scale, multi-physics phenomenon, a robust solver has

---

\* The work was partially supported by DOE DE-FC02-01ER25479 and DEFC02-04ER25595, and NSF ACI-0305666 and ACI-0352334.

to be applied in order to deal with the high degree of nonlinearity and the nonsmooth blowup behavior in the system. One of the successful approaches to the numerical solution of the MHD system is based on the splitting of the system into two parts, where equations for the current and the vorticity are advanced in time, and the corresponding potentials are obtained by solving Poisson equations in a separate step. In such an explicit approach, to satisfy the CFL condition, the time step may become very small, especially in the case of fine meshes, and the Poisson solves must therefore be performed frequently. On the other hand, implicit time stepping presents an alternative approach that may allow the use of larger time steps. However, the non-smooth nature of the solution often results in convergence difficulties. In this work we take a fully coupled approach such that no operator splitting is applied to the system of MHD equations. More precisely, we first apply a third-order implicit time integration scheme, and then, to guarantee nonlinear consistency, we use a one-level Newton-Krylov-Schwarz algorithm to solve the large sparse nonlinear system of algebraic equations containing all physical variables at every time step. The focus of this paper is on the convergence and parallel performance studies of the proposed implicit algorithm.

## 2 Model MHD Problem

We consider a model resistive MHD problem described as follows[2, 7]:

$$\left\{ \begin{array}{l} \nabla^2 \phi = U \\ \nabla^2 \psi = \frac{1}{d_e^2}(\psi - F) \\ \frac{\partial U}{\partial t} + [\phi, U] = \frac{1}{d_e^2}[F, \psi] + \nu \nabla^2 U \\ \frac{\partial F}{\partial t} + [\phi, F] = \rho_s^2[U, \psi] + \eta \nabla^2(\psi - \psi^0), \end{array} \right. \quad (1)$$

where  $U$  is the vorticity,  $F$  is the canonical momentum,  $\phi$  and  $\psi$  are the stream functions for the vorticity and current density, respectively,  $\nu$  is the plasma viscosity,  $\eta$  is the normalized resistivity,  $d_e = c/\omega_{pe}$  is the inertial skin depth, and  $\rho_s = \sqrt{T_e/T_i}\rho_i$  is the ion sound Larmor radius. The current density is obtained by  $J = (F - \psi)/d_e^2$ . The Poisson bracket is defined as:  $[A, B] \equiv (\partial A/\partial x)(\partial B/\partial y) - (\partial A/\partial y)(\partial B/\partial x)$ . Every variable in the system is assumed to be the sum of an equilibrium and a perturbation component; i.e.  $\phi = \phi^0 + \phi^1$ ,  $\psi = \psi^0 + \psi^1$ ,  $U = U^0 + U^1$ , and  $F = F^0 + F^1$ , where  $\phi^0 = U^0 = 0$ ,  $\psi^0 = \cos(x)$ , and  $F^0 = (1 + d_e^2) \cos(x)$  are the equilibrium components. After substitutions, we arrive at the following system for the perturbed variables:

$$\left\{ \begin{array}{l} \nabla^2 \phi^1 = U^1 \\ \nabla^2 \psi^1 = \frac{1}{d_e^2} (\psi^1 - F^1) \\ \frac{\partial U^1}{\partial t} + [\phi^1, U^1] = \frac{1}{d_e^2} [F^1, \psi^1] + \nu \nabla^2 U^1 + \frac{1}{d_e^2} \left( \frac{\partial \psi^1}{\partial y} F_{eqx} + \frac{\partial F^1}{\partial y} B_{eqy} \right) \\ \frac{\partial F^1}{\partial t} + [\phi^1, F^1] = \rho_s^2 [U^1, \psi^1] + \eta \nabla^2 \psi^1 + \left( \frac{\partial \phi^1}{\partial y} F_{eqx} + \rho_s^2 \frac{\partial U^1}{\partial y} B_{eqy} \right), \end{array} \right. \quad (2)$$

where  $F_{eqx} = -(1 + d_e^2) \sin(x)$  and  $B_{eqy} = \sin(x)$ . The system is defined on a rectangular domain  $\Omega \equiv [l_x, l_y] \equiv [2\pi, 4\pi]$ , and doubly periodic boundary conditions are assumed. For initial conditions, we use a nonzero initial perturbation in  $\phi^1$  and a zero initial perturbation in  $\psi^1$ . The exact form of the perturbation follows after some useful definitions. The aspect ratio is  $\epsilon = l_x/l_y$ . The perturbation's magnitude is scaled by  $\delta = 10^{-4}$ . We define  $\tilde{d}_e = \max\{d_e, \rho_s\}$  and  $\gamma = \epsilon \tilde{d}_e$ . For the initial value of the  $\phi$  perturbation we use

$$\phi^1(x, y, 0) = \begin{cases} \delta \frac{\gamma}{\epsilon} \operatorname{erf}\left(\frac{x}{\sqrt{2}\tilde{d}_e}\right) \sin(\epsilon y) & \text{if } 0 \leq x < \frac{\pi}{2} \\ -\delta \frac{\gamma}{\epsilon} \operatorname{erf}\left(\frac{x - \pi}{\sqrt{2}\tilde{d}_e}\right) \sin(\epsilon y) & \text{if } \frac{\pi}{2} \leq x < \frac{3\pi}{2} \\ \delta \frac{\gamma}{\epsilon} \operatorname{erf}\left(\frac{x - 2\pi}{\sqrt{2}\tilde{d}_e}\right) \sin(\epsilon y) & \text{if } \frac{3\pi}{2} \leq x \leq 2\pi. \end{cases} \quad (3)$$

Other quantities are set as:  $U^1(x, y, 0) = \nabla^2 \phi^1(x, y, 0)$  and  $F^1(x, y, 0) = \psi^1(x, y, 0) - d_e \nabla^2 \psi^1(x, y, 0)$ . From now on, we drop the superscript and assume that the four fields  $\phi$ ,  $\psi$ ,  $U$  and  $F$  represent the perturbed components only. In order to connect the stream functions to physical quantities the following definitions are used:  $\mathbf{v} = e_z \times \nabla \phi$  and  $\mathbf{B} = B_0 e_z + \nabla \psi \times e_z$ . Here  $\mathbf{B}$  stands for the total magnetic field,  $B_0$  is the guiding field in the  $z$  direction, and  $\mathbf{v}$  is the velocity in the plane perpendicular to the guiding field.

We discretize the system of PDEs with finite differences on a uniform mesh of sizes  $h_x$  and  $h_y$  in  $x$  and  $y$  directions, respectively. At time level  $t^k$ , we denote the grid values of the unknown functions  $\phi(x, y, t)$ ,  $\psi(x, y, t)$ ,  $U(x, y, t)$ , and  $F(x, y, t)$ , as  $\phi_{i,j}^k$ ,  $\psi_{i,j}^k$ ,  $U_{i,j}^k$ , and  $F_{i,j}^k$ . The time independent components of the system (2) are discretized with the standard second-order central difference method. For the time discretization, we use some multistep formulas, known as backward differentiation formulas (BDF) [8]. In this paper, we focus on a third-order temporal and second-order spatial discretizations as shown in (4), where  $R_\phi^{k+1}(i, j)$ ,  $R_\psi^{k+1}(i, j)$ ,  $R_U^{k+1}(i, j)$ , and  $R_F^{k+1}(i, j)$  are the second-order accurate spatial discretizations of the time-independent components. We need to know solutions at time steps  $k-2$ ,  $k-1$  and  $k$  in order to compute a solution at time step  $k+1$  in (4). A lower order scheme (second-order backward Euler) is employed at the beginning of the time integration for these start-up values.

$$\begin{cases} R_\phi^{k+1}(i, j) = 0 \\ R_\psi^{k+1}(i, j) = 0 \\ \frac{h_x h_y}{6\Delta t} (11U_{i,j}^{k+1} - 18U_{i,j}^k + 9U_{i,j}^{k-1} - 2U_{i,j}^{k-2}) - R_U^{k+1}(i, j) = 0 \\ \frac{h_x h_y}{6\Delta t} (11F_{i,j}^{k+1} - 18F_{i,j}^k + 9F_{i,j}^{k-1} - 2F_{i,j}^{k-2}) - R_F^{k+1}(i, j) = 0 \end{cases} \quad (4)$$

### 3 One-level Newton-Krylov-Schwarz Method

At each time step, the discretized fully coupled system (4) is solved with a one-level Newton-Krylov-Schwarz algorithm (NKS). NKS is a general purpose parallel algorithm for solving systems of nonlinear algebraic equations. NKS has three main components: an inexact Newton algorithm, a Krylov subspace linear solver, and an additive Schwarz preconditioner. At each time step, the discretized system of equations can be represented by  $G(E) = 0$ , where  $E = \{\phi, \psi, U, F\}$ . The unknowns are ordered mesh point by mesh point, and at each mesh point they are in the order  $\phi$ ,  $\psi$ ,  $U$ , and  $F$ . The mesh points are ordered subdomain by subdomain for the purpose of parallel processing. The Newton iteration is given as:  $E_{k+1} = E_k - \lambda_k J(E_k)^{-1} G(E_k)$ ,  $k = 0, 1, \dots$ , where  $E_0$  is a solution obtained at the previous time step,  $J(E_k) = G'(E_k)$  is the Jacobian at  $E_k$ , and  $\lambda_k$  is the steplength determined by a linesearch procedure [4]. Due to doubly periodic boundary conditions, the Jacobian has a one-dimensional null-space that is removed by projecting out a constant. In the inexact Newton's method we do not solve the Jacobian system exactly. The accuracy of the Jacobian solver is determined by some  $\eta_k \in [0, 1)$  and the condition  $\|G(E_k) + J(E_k)s_k\| \leq \eta_k \|G(E_k)\|$ . The overall algorithm can be described as follows:

1. Inexactly solve the linear system  $J(E_k)s_k = -G(E_k)$  for  $s_k$  using a preconditioned GMRES(30) [11].
2. Perform a full Newton step with  $\lambda_0 = 1$  in the direction  $s_k$ .
3. If the full Newton step is unacceptable, backtrack  $\lambda_0$  using a backtracking procedure until a new  $\lambda$  is obtained that makes  $E_+ = E_k + \lambda s_k$  an acceptable step.
4. Set  $E_{k+1} = E_+$ , go to step 1 unless a stopping condition has been met.

In step 1 above we use a left-preconditioned GMRES to solve the linear system; i.e., the vector  $s_k$  is obtained by approximately solving the linear Jacobian system  $M_k^{-1} J(E_k)s_k = -M_k^{-1} G(E_k)$ , where  $M_k^{-1}$  is a one-level additive Schwarz preconditioner. To formally define  $M_k^{-1}$ , we need to introduce a partition of  $\Omega$ . We first partition the domain into non-overlapping substructures  $\Omega_l$ ,  $l = 1, \dots, N$ . In order to obtain an overlapping decomposition of the domain, we extend each subregion  $\Omega_l$  to a larger region  $\Omega'_l$ , i.e.,  $\Omega_l \subset \Omega'_l$ . Only simple box decomposition is considered in this paper – all the subdomains  $\Omega_l$  and  $\Omega'_l$  are rectangular and made up of integral numbers of fine mesh cells.

The size of  $\Omega_l$  is  $H_x \times H_y$  and the size of  $\Omega'_l$  is  $H'_x \times H'_y$ , where the  $H'$ 's are chosen so that the overlap,  $ovlp$ , is uniform in the number of fine grid cells all around the perimeter, i.e.,  $ovlp = (H'_x - H_x)/2 = (H'_y - H_y)/2$  for interior subdomains. For boundary subdomains, we simply cut off the part that is outside  $\Omega$ . On each extended subdomain  $\Omega'_l$ , we construct a subdomain preconditioner  $B_l$ , whose elements are  $B_l^{i,j} = \{J_{ij}\}$ , where the node indexed by  $(i, j)$  belongs to  $\Omega'_l$ . The entry  $J_{ij}$  is calculated with finite differences  $J_{ij} = 1/(2\delta)(G_i(E_j + \delta) - G_i(E_j - \delta))$ , where  $0 < \delta \ll 1$  is a constant. Homogeneous Dirichlet boundary conditions are used on the internal subdomain boundary  $\partial\Omega'_l \cap \Omega$ , and the original boundary conditions are used on the physical boundary, if present. The additive Schwarz preconditioner can be written as

$$M_k^{-1} = (R_1)^T B_1^{-1} R_1 + \dots + (R_N)^T B_N^{-1} R_N. \quad (5)$$

Let  $n$  be the total number of mesh points and  $n'_l$  the total number of mesh points in  $\Omega'_l$ . Then,  $R_l$  is an  $n'_l \times n$  block matrix that is defined as: its  $4 \times 4$  block element  $(R_l)_{i,j}$  is an identity block if the integer indices  $1 \leq i \leq n'_l$  and  $1 \leq j \leq n$  belong to a mesh point in  $\Omega'_l$ , or a block of zeros otherwise. The  $R_l$  serves as a restriction matrix because its multiplication by a block  $n \times 1$  vector results in a smaller  $n'_l \times 1$  block vector by dropping the components corresponding to mesh points outside  $\Omega'_l$ . Various inexact additive Schwarz preconditioners can be constructed by replacing the matrices  $B_l$  in (5) with convenient and inexpensive to compute matrices, such as those obtained with incomplete factorizations. In this paper we employ the *ILU* factorization.

## 4 Numerical Results

To illustrate model behavior, we choose nominal values of the inertial skin depth  $d_e = 0.08$  and the ion sound Larmor radius  $\rho_s = 0.24$ . The normalized resistivity and viscosity are chosen in the range  $\eta, \nu \in [10^{-4}, 10^{-2}]$ . Time in the system is normalized to the Alfvén time  $\tau_A = \sqrt{4\pi n m_i l_x} / B_{y0}$ , where  $B_{y0}$  is the characteristic magnitude of the equilibrium magnetic field and  $l_x$  is the macroscopic scale length [7].  $\Omega$  is uniformly partitioned into rectangular meshes up to  $500 \times 500$  in size. The stopping conditions for the iterative processes are given as follows: relative reduction in nonlinear function norm  $\|G(E_k)\| \leq 10^{-2} \|G(E_0)\|$ , absolute tolerance in nonlinear function norm  $\|G(E_k)\| \leq 10^{-10}$ , relative reduction in linear residual norm  $\|r_k\| \leq 10^{-6} \|r_0\|$ , and absolute tolerance in linear residual norm  $\|r_k\| \leq 10^{-10}$ .

A typical solution is shown in Fig.1. The initial perturbation in  $\phi$  produces a feature-rich behavior in  $\psi$ ,  $U$ , and  $F$ . The four variables in the system evolve at different rates:  $\phi$  and  $\psi$  evolve at a slower rate than  $F$  and  $U$ . For  $\eta = 10^{-3}$  and  $\nu = 10^{-3}$  we observe an initial slow evolution of current density profiles up to time  $100\tau_A$  and the solution blows up at time near  $250\tau_A$ . In the middle of the domain the notorious “X” structure is developed, as can be seen in the  $F$

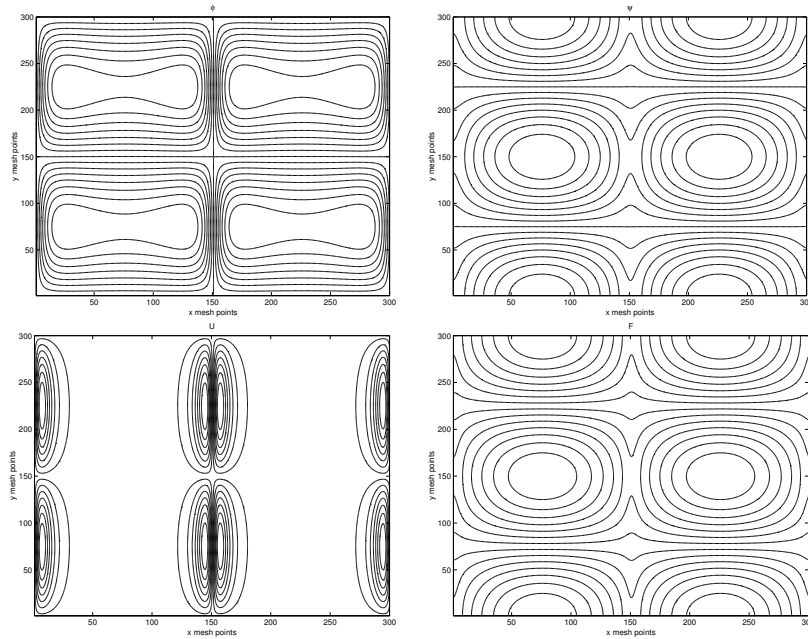


**Fig. 1.** Contour plots of  $\phi$  (top left),  $\psi$  (top right),  $U$  (bottom left), and  $F$  (bottom right). The results are obtained on  $300 \times 300$  mesh,  $\Delta t = 1.0\tau_A$ ,  $t = 100\tau_A$ ,  $\eta = 10^{-3}$ ,  $\nu = 10^{-3}$ , implicit time stepping.

contours, where the magnetic flux is being reconnected. Similar reconnection areas are developed on the boundaries of the domain due to the periodicity of boundary conditions and the nature of the initial  $\phi$  perturbation. In the reconnection regions, sharp current density peaks (Fig. 2 (a)) are formed. We compare results obtained by our implicit method with these obtained with an explicit method [5]. Fig. 2 (b) shows that the third-order implicit method allows for much larger time steps, and still produces results that are very close to these obtained with the explicit algorithm, where the size of the time step is determined by the CFL constraint.

Next, we look at some of the machine dependent properties of the algorithm. Our main concern is the scalability, which is an important quality in evaluating parallel algorithms. First, we look at the total computing time as a function of the number of subdomains and calculate  $t(1)/t(np)$  which gives a ratio of time needed to solve the problem with one processor to the time needed to solve the problem with  $np$  processors. Our experiments are conducted on a Linux cluster. Fig.3 shows the results for a  $500 \times 500$  mesh, and overlap 1 is used in all cases. We can see that the one-level algorithm scales reasonably well in terms of the total computing time. Table 1 illustrates results obtained on a  $300 \times 300$  mesh. The time scalability is attained despite the fact that the total number of linear iterations increases with the number

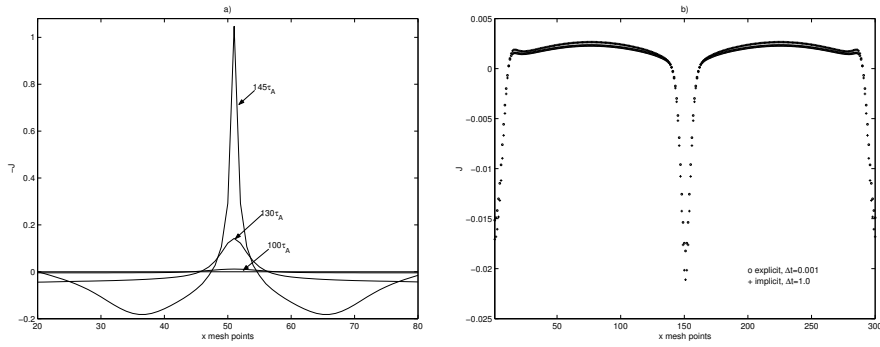


**Fig. 2.** a) Formation of current density peaks in the reconnection region,  $J$ ,  $100 \times 100$  mesh,  $\eta = 10^{-2}$ ,  $\nu = 10^{-2}$ ,  $\Delta t = 1.0\tau_A$ . b) Comparison plots of  $J$  obtained with the explicit method ( $\Delta t = 0.001\tau_A$ ) and the implicit with  $\Delta t = 1.0\tau_A$  at  $t = 200\tau_A$  on  $300 \times 300$  mesh with  $\eta = 10^{-3}$  and  $\nu = 10^{-3}$ .

of subdomains. Interestingly enough, the total number of nonlinear iterations decreases with the increase of the number of subdomains.

**Table 1.** Scalability with respect to the number of processors,  $300 \times 300$  mesh. ILU factorization for all subproblems,  $ovlp = 1$ . Time step  $\Delta t = 1.0\tau_A$ , 10 time steps,  $t = 100\tau_A$ . The problem is solved with 64, 32, 16, 8, 16, 8, 4 and 1 processors.

$np$	$t$ [sec]	Total Nonlinear	Total Linear	Linear/Nonlinear
1	4846	19	4865	256
2	3009	19	4938	260
4	1943	12	6444	537
8	1345	14	8596	614
16	892	16	19923	808
32	350	11	7541	686
64	275	11	9754	887

## 5 Conclusions and Future Work

The proposed fully coupled implicit scheme with a third-order time discretization allows much larger time steps than the explicit method, while still preserving the solution accuracy. One-level NKS converges well with the problem parameters in the specified range, given the right stopping conditions. Without a coarse space, the algorithm scales reasonably well for medium number of processors with a small subdomain overlap. Future continuation of this work may include solutions of the MHD problem on finer meshes with a larger number of processors. Longer time integration with various  $\eta$  and  $\nu$  values, as

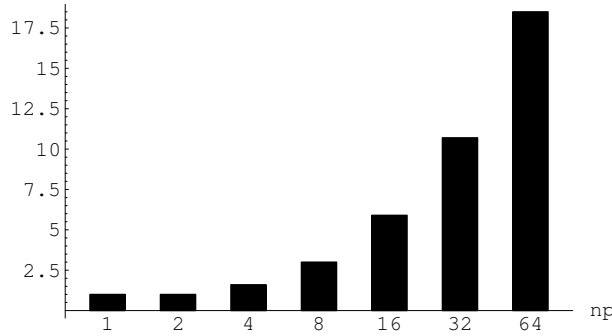


**Fig. 3.** Computing time scalability  $t(1)/t(np)$ ,  $500 \times 500$  mesh,  $\eta = 10^{-3}$ ,  $\nu = 10^{-3}$ ,  $\Delta t = 0.1\tau_A$  with 1 – 64 processors,  $t = 100\tau_A$ . The data are collected over 100 time steps.

well as higher  $\rho_s$  to  $d_e$  ratios, may be helpful in the further understanding of the algorithm for the numerical solutions of MHD problems.

## References

1. Balay S., Buschelman K., Gropp W.D., Kaushik D., Knepley M., McInnes L.C., Smith B.F., and Zhang H., *PETSc Users Manual*, ANL-95/11 - Revision 2.1.5, Argonne National Laboratory, (2002)
2. Cafaro E., Grasso D., Pegoraro F., Porcelli F., Saluzzi A., *Invariants and geometric structures in nonlinear Hamiltonian magnetic reconnection*, Phys. Rev. Let., **80**(20), 4430–4433, (1998)
3. Chacon L., Knoll D.A., Finn J.M., *An implicit, nonlinear reduced resistive MHD solver*, J. Comput. Phys., **178**, 15–36, (2002)
4. Dennis J.E. and Schnabel R.B., *Numerical Methods for Unconstrained Optimization and Nonlinear Equations*, SIAM, Philadelphia, (1996)
5. Germaschewski K., *personal communications*
6. Goldston R.J., Rutherford P.H., *Introduction to Plasmas Physics*, IOP Publishing, (1995)
7. Grasso D., Pegoraro F., Porcelli F., Califano F., *Hamiltonian magnetic reconnection*, Plasma Phys. Control Fusion, **41**, 1497–1515, (1999)
8. Hairer E., Norsett S.P., and Wanner G., *Solving Ordinary Differential Equations I*, Springer-Verlag, (1991)
9. Ottaviani M., Porcelli F., *Nonlinear collisionless magnetic reconnection*, Phys. Rev. Let., **71**(23), 3802–3805, (1993)
10. Ottaviani M., Porcelli F., *Fast nonlinear magnetic reconnection*, Phys. Plasmas, **2**(11), 4104–4117, (1995)
11. Saad Y., *Iterative Methods for Sparse Linear Systems*, SIAM (2003)
12. Strauss H.R., Longcope D.W., *An adaptive finite element method for magneto-hydrodynamics*, J. Comput. Phys., **147**, 318–336, (1998)